Supplements

ECE3p5 model

This suppelement shows some additional information on the temperature and the geopotential height as simulated by the ECE3p5 climate model. In Figure S1, the Northern Hemisphere zonal mean bias of the temperature and the ECE3p5 temperature bias compared to ERA5 is shown. In Figure S2, the annual Z500 bias of ECE3p5 compared to ERA5 reanalysis data is shown, and in Figure S3, the spatial bias in the geopotential height gradient is shown. Figure S1 can be compared to Figure 4 and 5 from (Döscher et al., 2022), where the same analysis is done for ECE3. In Figure S4, the model variability between the 16 ensemble members is shown.

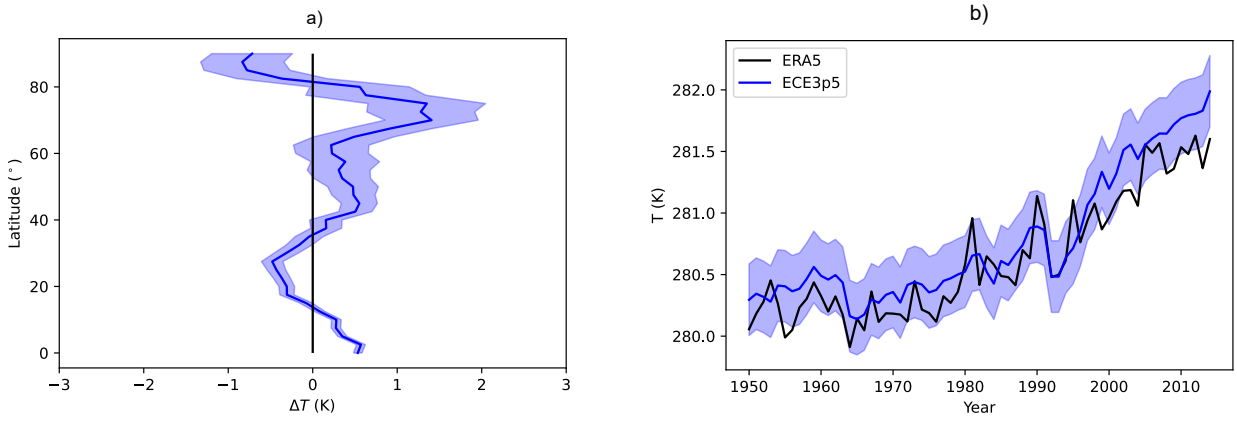

Figure S1. a) NH zonal mean bias in TAS (K). b) NH annual mean TAS (K), ECE3p5 model (blue line) temperature bias on the NH compared to ERA5 (black lines) over 1950-2014. Blue shade shows one standard deviation (σ) of the variability over the 16 ensembles in ECE3p5 for both a) and b).

Blocking index

In this supplement, a timeslide of the seasonality of the absolute propagation velocity is shown over the years in Figure S5. From this figure we can see that there are no clear changes in the propagation velocity over the time period of 1850-2014 over all 16 ensembles, allowing us to use the whole dataset in our analysis. In Figure S6 and S7 the blocking frequency and spatial distribution are shown for the minimum blocking latitude used by (Sousa et al., 2021) when all blocks are taken into account. Because these blocks are situated mostly close to the fixed minimum blocking latitude, we chose to use a variable minimum latitude.

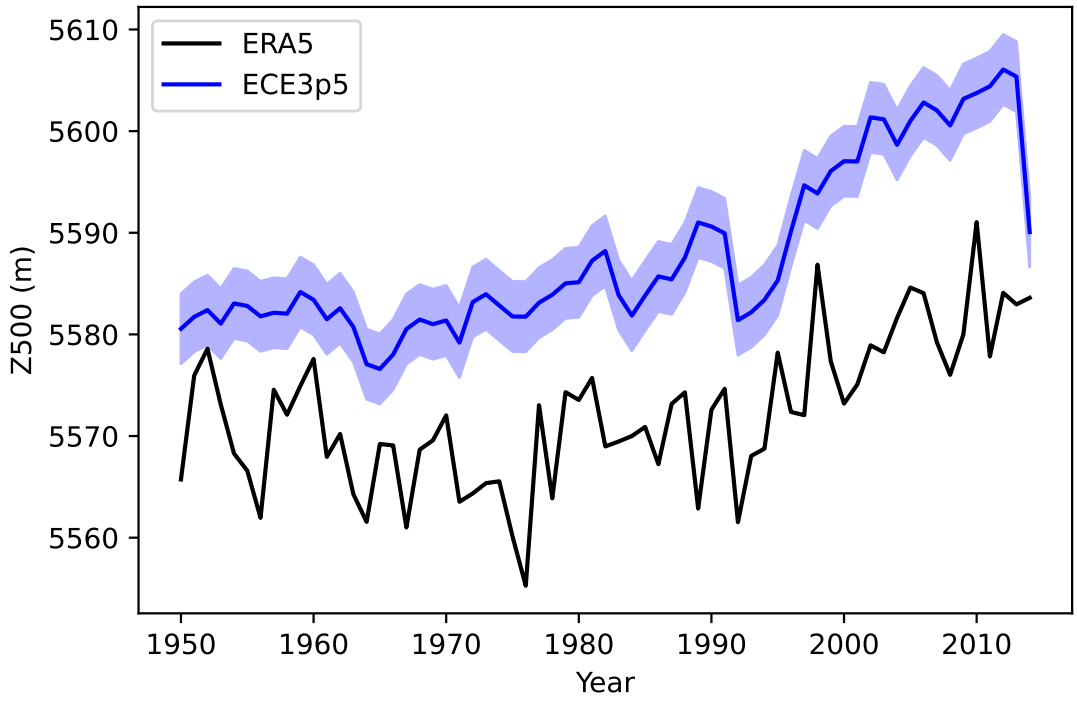

Figure S2. NH annual mean Z500 (m) for ERA5 (black) and ECE3p5 (blue) over the period of 1950-2014. Blue shading represents one standard deviation (σ) of the 16 ensemble variability.

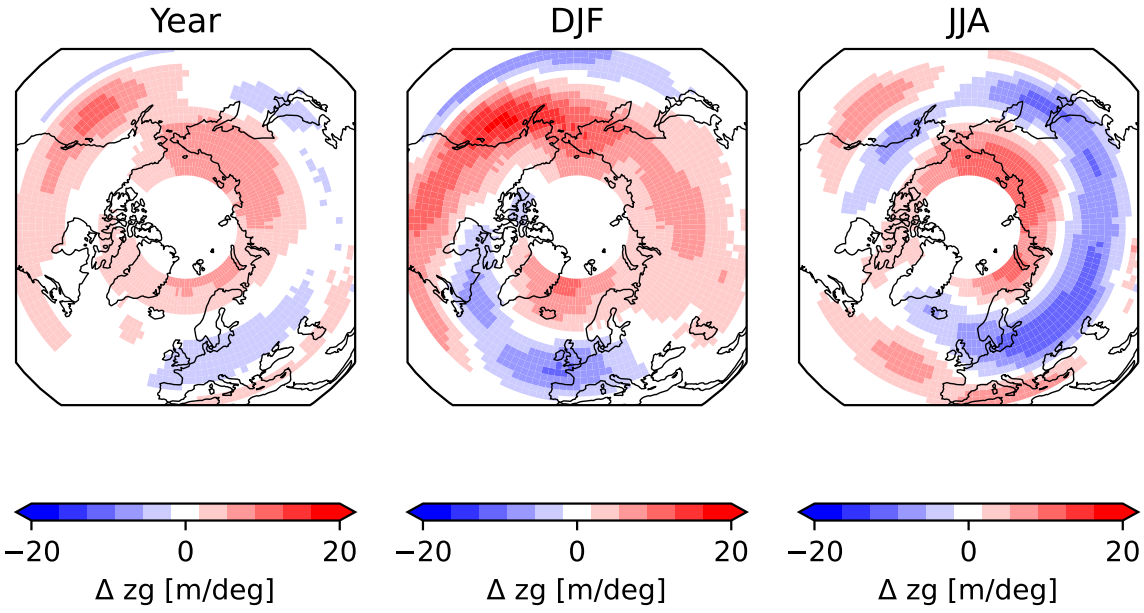

Figure S3. Difference between the gradient in Z500 for ECE3p5 and ERA5 over the period of 1951-2014 over all 16 ensemble members. Red is overestimation by the model, blue is underestimation by the model.

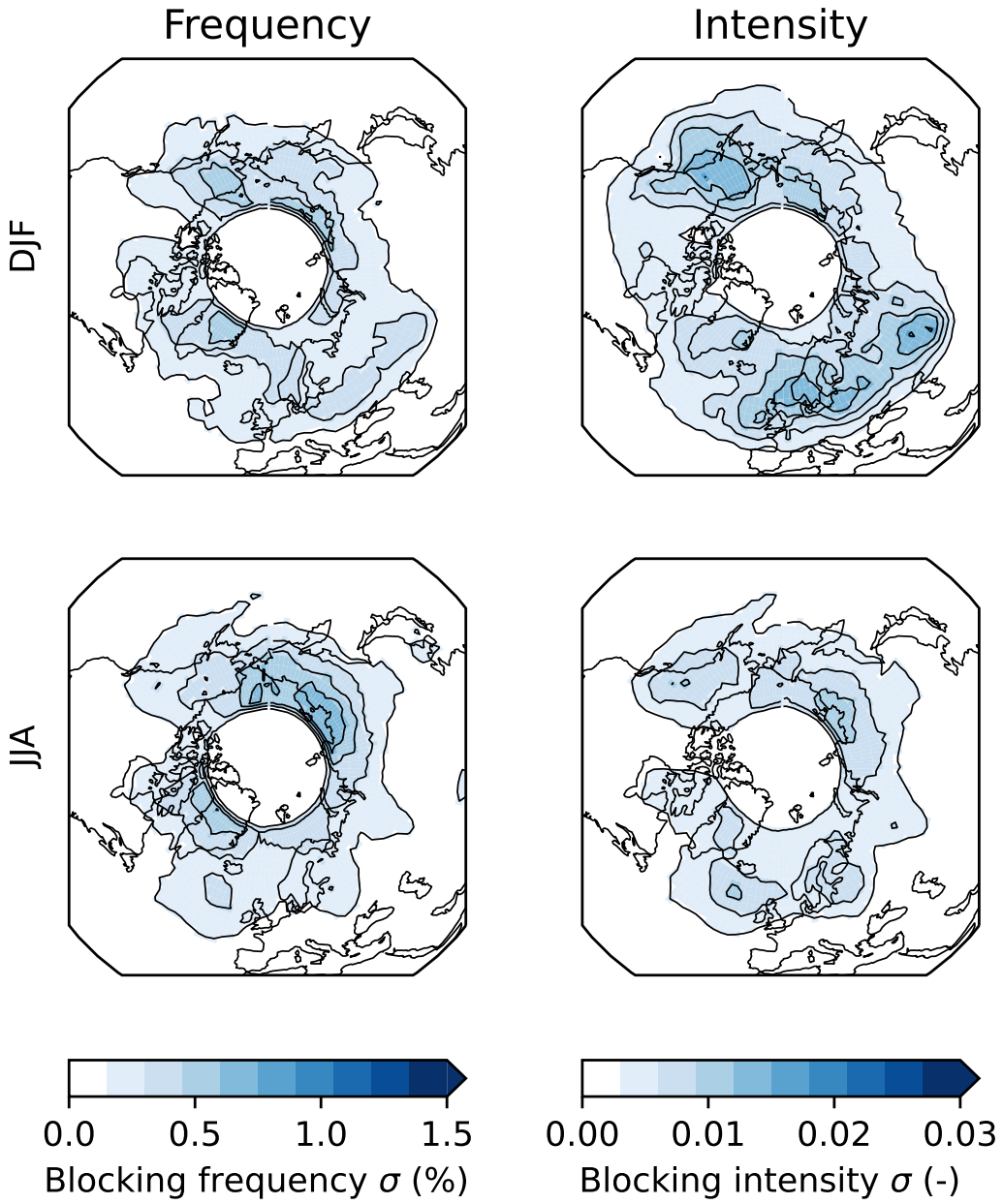

Figure S4. Standard deviation of climatological blocking frequency (left) and blocking intensity (right), for the winter season (DJF, upper row) and summer season (JJA, lower row). The standard deviation shows the variability between the 16 ensemble members of ECE3p5 over the whole historical dataset, running from 1850-2014.

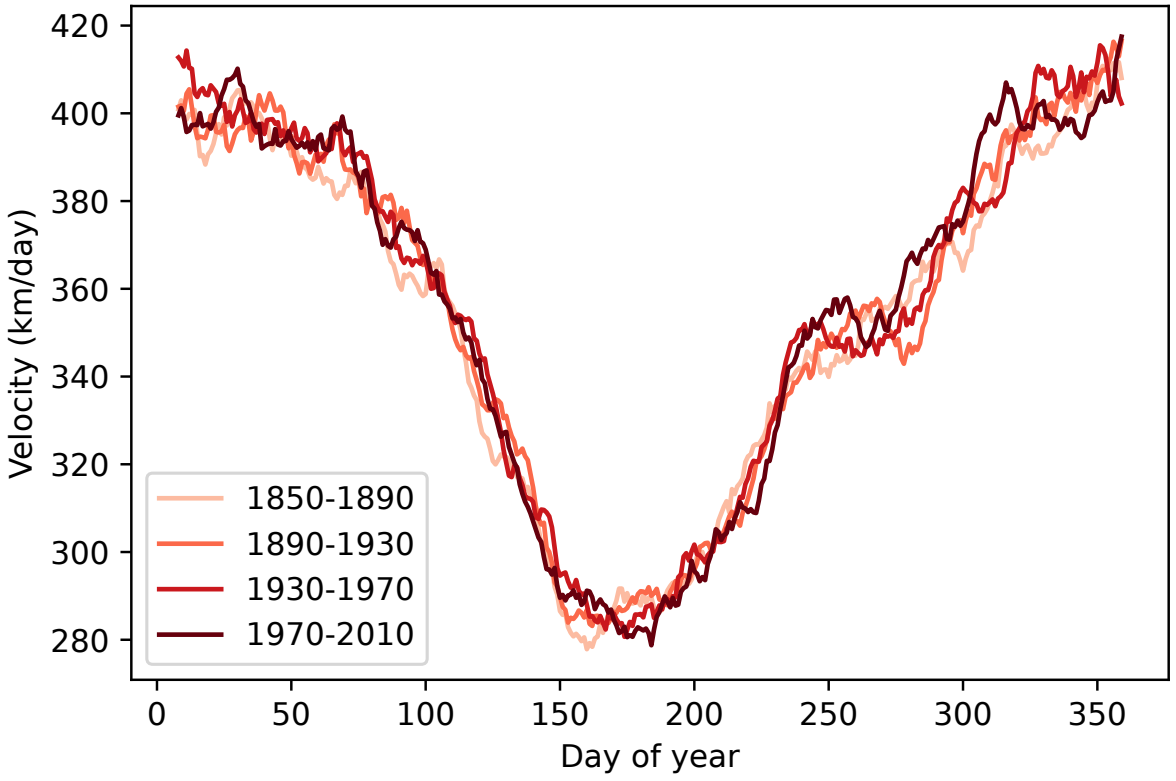

Figure S5. Timeslide of the absolute mean propagation velocity per day of the year for the ECE3p5 dataset from 1850-2014 over all 16 ensemble members.

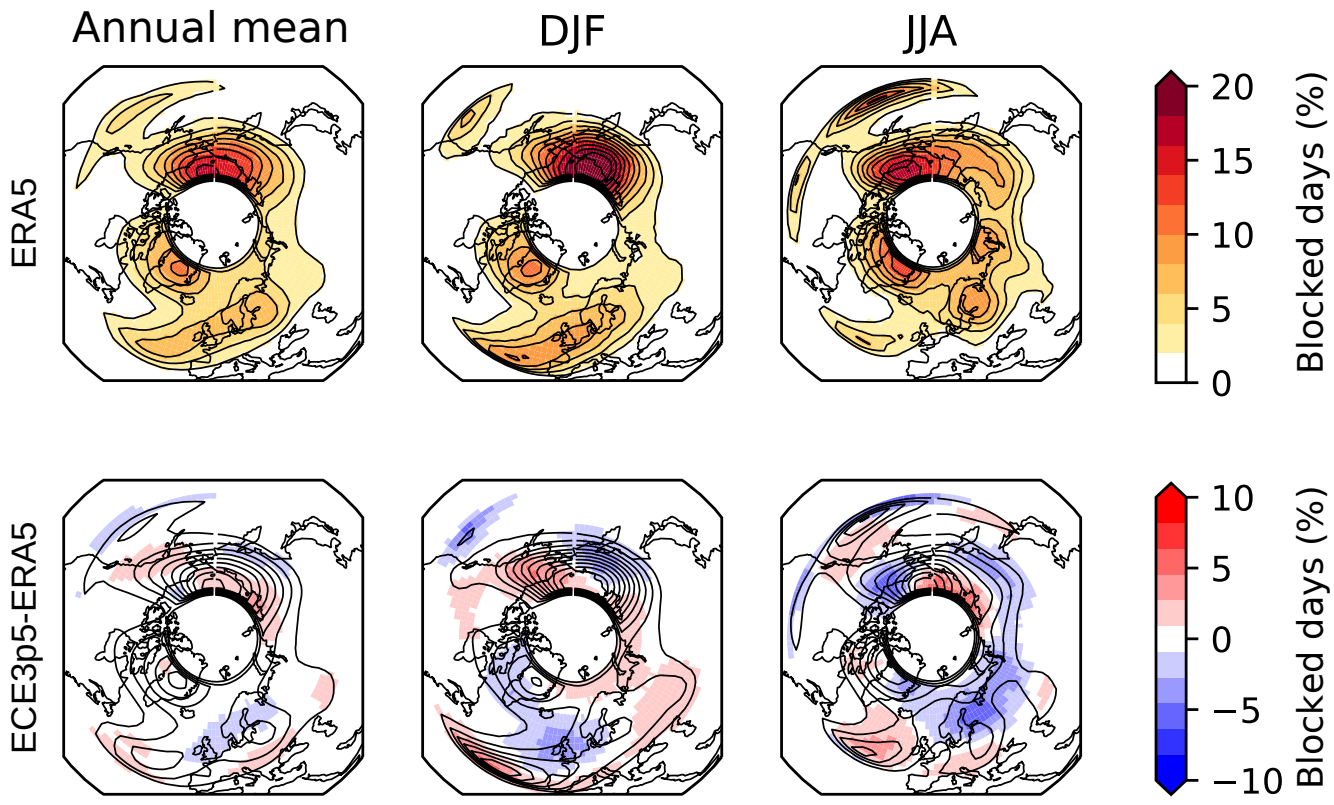

Figure S6. Upper row: Climatological blocking intensity ERA5 (contours and shading) for the annual mean, winter mean (DJF), and summer mean (JJA). Lower row: contours show blocking intensity of ECE3p5, shading shows the difference between ERA5 and ECE3p5 for the annual mean, winter mean, and summer mean. Both the data from ERA5 and ECE3p5 are taken over the period of 1951-2014. Instead of the variable minimum latitude which was used in the paper and in Figure 2, here the minimum blocking latitude of Sousa et al. (2021) is used.

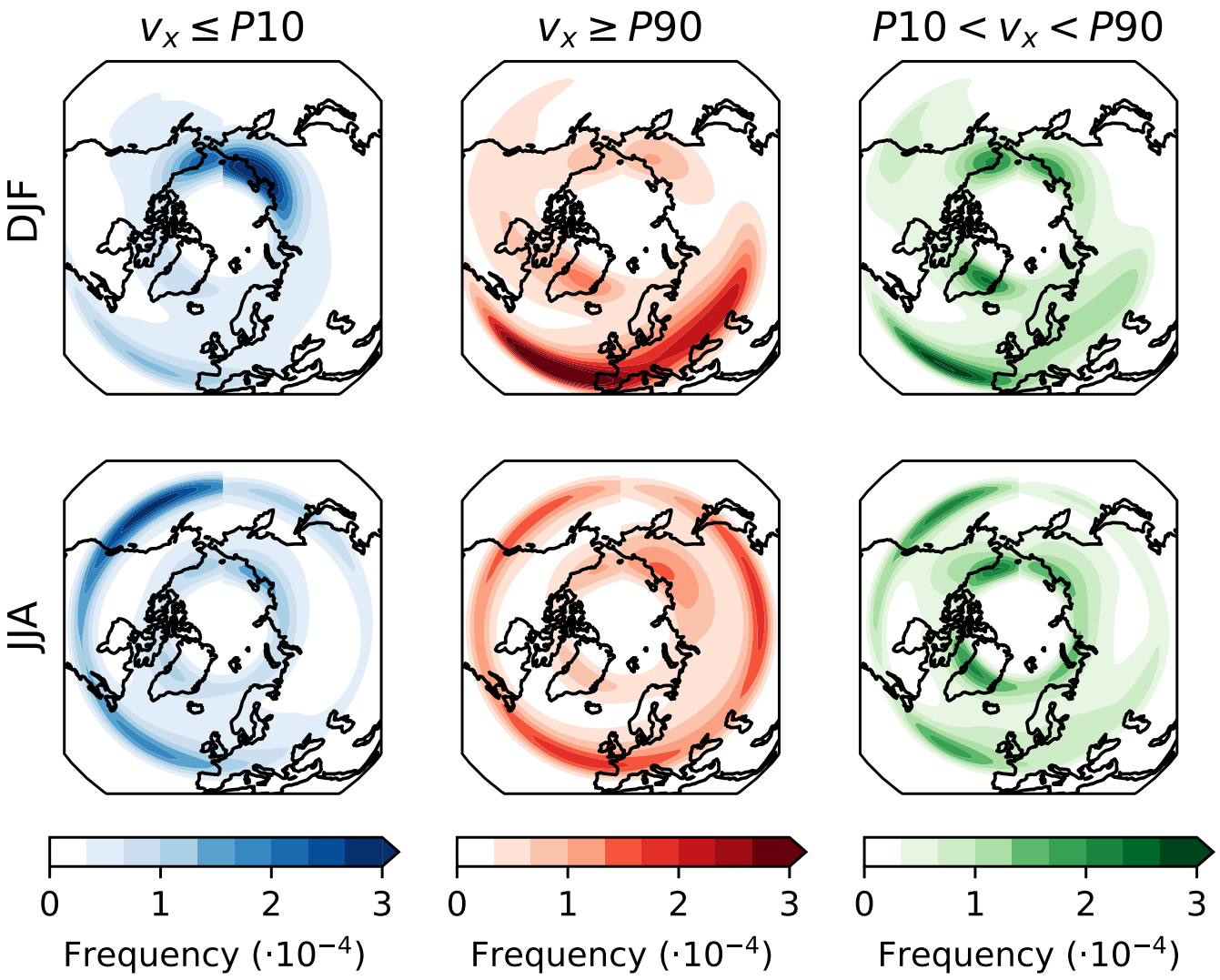

Figure S7. Spatial distribution weighted (based on BI) blocking centres, on the fourth day. First column: the 10% fastest westward-moving blocks ($v_x \leq P10$). Middle column: the 10% fastest eastward-moving blocks ($v_x \geq P90$). Third column: all propagation velocities in between ($P10 < v_x < P90$). All taken separately over all winter months (DJF, upper row) and over all summer months (JJA, lower row) over the period of 1850-2014 for all 16 ensembles of ECE3p5. Instead of the variable minimum latitude which was used in the paper and in Figure 6, here the minimum blocking latitude of Sousa et al. (2021) is used.

Temperature anomalies associated with the propagation velocity

In Section 3.5, the lower-right quadrant of the area around the block was shown. Here we show the other three quadrants for completion.

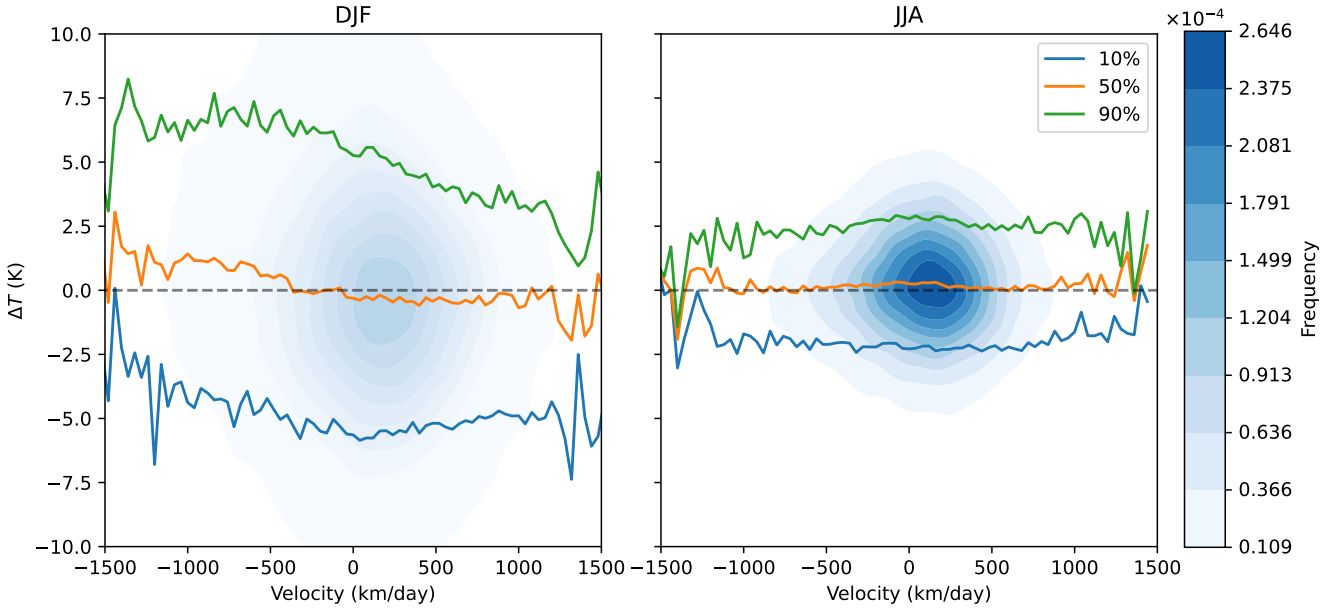

Figure S8. Kernel density estimation (blue shading) and the 10^{th} (blue), 50^{th} (orange) and 90^{th} (green) percentiles of the lower-left quadrant of the 2m temperature anomaly plotted against the propagation velocity, all for winter (DJF, left) and summer (JJA, right). Only temperature anomalies over land are taken into account. Taken over the period of 1950-2014 over all 16 ensemble members of ECE3p5.

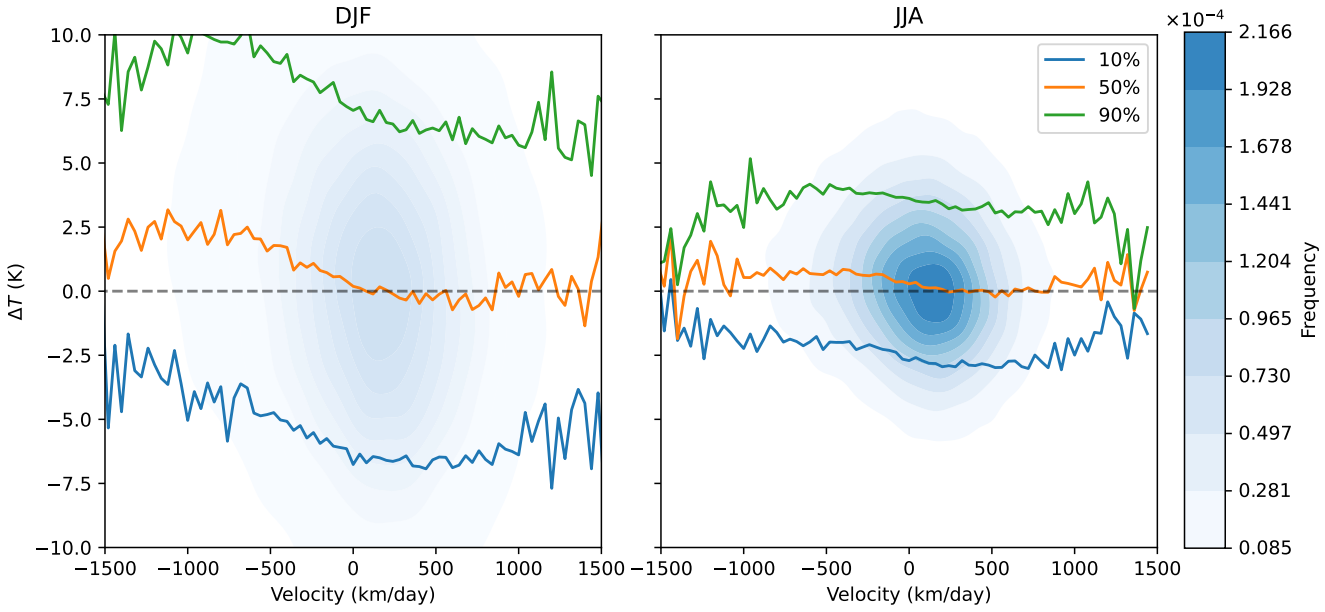

Figure S9. As in Figure S8 but for the upper-right quadrant.

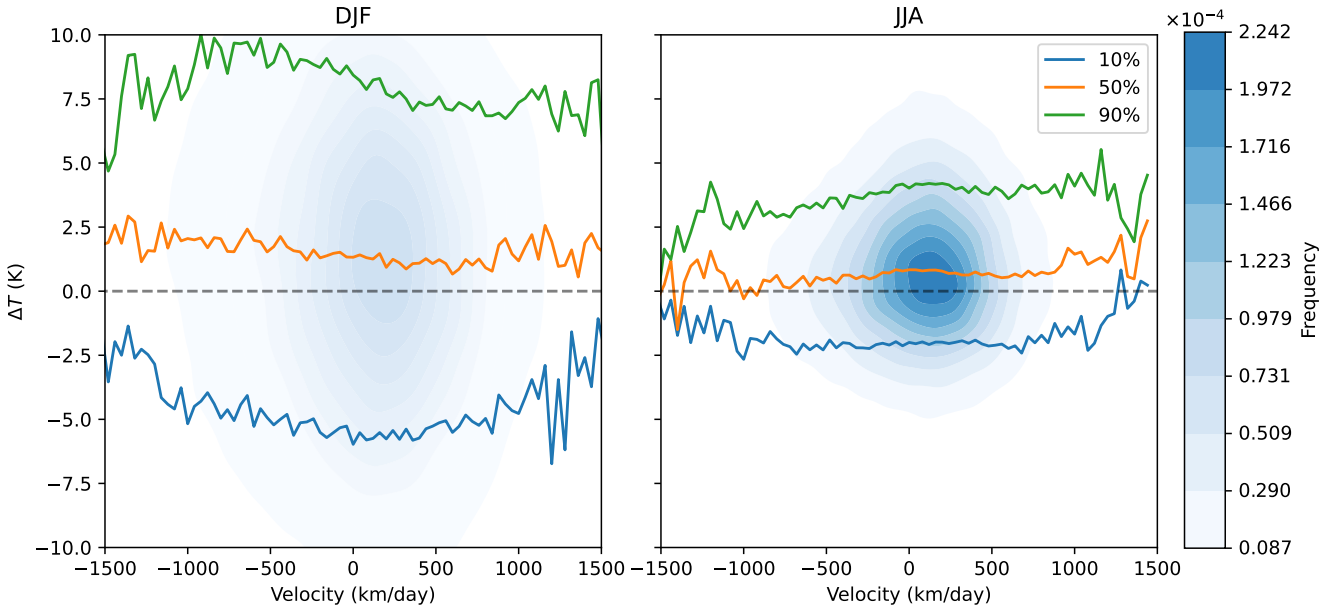

Figure S10. As in Figure S8 but for the upper-left quadrant.